Materials Advances

ROYAL SOCIETY OF CHEMISTRY

PAPER

View Article Online
View Journal | View Issue

Cite this: *Mater. Adv.*, 2025, 6, 670

Analysis of Pb(II) in wheat grain, cow urine and squid samples using modified novel TSDB incorporated MWCNTs

Jayagopi Gayathri, *[a] Sivakumar Sivalingam [a] and Kumar Sangeetha Selvan *[b]

Received 28th August 2024,
Accepted 21st November 2024

DOI: 10.1039/d4ma00857j

rsc.li/materials-advances

To fabricate a selective lead (Pb(II)) ion sensor, a slurry of the synthesized *N*,*N*′,*N*″,*N*‴-tetrasalicylidene-3,3′-diaminobenzidine (TSDB) ligand was deposited on multiwalled carbon nanotubes (MWCNTs)/paraffin graphite electrode (PGE). The ligand (octadentate) was easily synthesized using 3,3′-diaminobenzidine and salicylaldehyde. The TSDB ligand that was synthesized was verified using Fourier transform infrared (FT-IR) spectroscopy, proton nuclear magnetic resonance (^{1}H-NMR) spectroscopy and carbon-13 nuclear magnetic resonance (^{13}C-NMR) spectroscopy. Scanning electron microscopy (SEM) and energy dispersive X-ray spectroscopy (EDAX) were used to analyze the surface morphology of Pb(II)-TSDB/MWCNTs/PGE, TSDB/MWCNTs/PGE, MWCNTs/PGE, and PGE. TSDB/MWCNTs/PGE, MWCNTs/PGE, and PGE were confirmed for conductivity using cyclic voltammetry (CV) and electrochemical impedance spectroscopy (EIS). Pb(II) was examined using square wave anodic stripping voltammetry (SWASV) on TSDB/MWCNTs/PGE, MWCNTs/PGE, and PGE. Pb(II) stripping voltammetry was carried out using the TSDB/MWCNTs/PGE at varying concentrations (0.8–222 μg L^{-1}). It was found that the lowest detection limit was 0.15 μg L^{-1}. During sensing performances, the Pb(II) sensor with active TSDB exhibits stability, perfect reproducible results, interference, and stability. Above all, its successive applicability to the detection of squid, cow urine and wheat grain samples was demonstrated. Atomic absorption spectroscopy (AAS) measurements are correlated with those of the real samples.

1. Introduction

Ever-increasing amounts of toxic heavy metals are released into the environment, posing a threat to human health as they accumulate in soil and human beings. They are also a major problem since they are contaminants in garbage that is disposed of in outflows.[1] Pb(II) and its congeners are difficult to separate from one another and remain stable in soil for extended periods of time, which causes bioaccumulation in agricultural products and trophic transmission to humans.[2]

Even while plants take up a considerable amount of lead ions from the soil, only a small amount of the Pb(II) load moves from the roots to the stems and leaves.[3] Although heavy metals are present in large quantities in the Earth's crust, human activities like mining, smelting, burning coal, storing battery effluents, car exhaust, metal plating, tanning leather, finishing operations, and adding fertilizers, pesticides, and additives to paint, gasoline, and other products can enrich these substances in food and cause their contents to exceed safe limits.[4] As a result, the extensive use of Pb(II) in many regions of the world has given rise to many environmental issues as well as threats to human health.[5,6]

Vegetable and wheat plants are occasionally used to treat metal-contaminated soil and groundwater because they are efficient at removing metals from the Earth.[7] In commercial vegetable plant production, the application of metal-containing fertilizers, herbicides, lead arsenate, and other pesticides raises the metal Pb(II) content in cabbage leaves, which have a non-negligible Pb(II) concentration. Furthermore, Pb(II) is a well-known toxin that has been connected to numerous issues with human health.[8] Pb(II), for example, exhibits an impact on the neurological, reproductive, hematological, cardiovascular, and renal systems.[9–11]

There is a great tendency to develop selective and sensitive detection methods for controlling toxic heavy metal ions as a result of their significant hazard effect.[12] Many techniques, including atomic absorption/emission spectrometry,[13] X-ray fluorescence spectrometry (XFS)[14] and inductively coupled plasma mass spectrometry (ICP-MS)[15] are stable and therefore commonly used to determine Pb(II). However, the disadvantages of these techniques, including complex analytical procedures, expensive instruments, and lengthy sample processing, hinder their practical application. The exceptional sensitivity of square

[a] *Department of Chemistry, VelTech Rangarajan Dr. Sagunthala R & D Institute of Science and Technology, Avadi, Chennai, Tamil Nadu, 600 062, India. E-mail: drgayathrij@veltech.edu.in*
[b] *Department of Chemistry, Anna Adharsh College for Women, Anna Nagar, Chennai, Tamil Nadu, 600040, India. E-mail: msc.sangi@gmail.com*

wave anodic stripping voltammetry (SWASV), a traditional electrochemical technique, has drawn a lot of interest for the simultaneous study of several heavy metal ions.[16,17]

Currently, the development of improved electrode materials is a major factor influencing the sensitivity of SWASV. Over the past ten years, a variety of materials have been utilized as modifiers in the preparation of electrochemical sensors, including complexes,[18] nanomaterials,[19] carbon-based compounds,[20–24] and so forth. These modifiers help increase sensitivity, specific surface area, and conductivity, which make SWASV an attractive substitute for conventional analytical methods with a lower detection limit.[25–28]

Schiff bases are chemical compounds formed when a primary amine reacts with an aldehyde or a ketone to form an imine. Schiff bases can be easily altered by selecting the right amine and substituting a carbonyl molecule. The utility of ligands containing N and O donors lies in their rigidity, coplanarity, and bite angle, resulting in a wide range of structural diversity. Schiff bases are widely used in electrochemical applications owing to their characteristic structure and their ability to bind to electrode surfaces.[29]

The synthesis of TSDB, modification of the TSDB/MWCNTs/PGE, and evaluation of the electrochemical behavior of the TSDB/MWCNTs/PGE for Pb(II) sensing were carried out in this research work. The present work deals with the synthesis and characterization of an octadentae ligand, *N*,*N*′,*N*″,*N*‴-tetrasalicylidene-3,3′-diaminobenzidine (TSDB, Scheme 1), which bears two sets of N_2O_2 donor sites separated by a biphenylene group. To the best of our knowledge, no one has yet demonstrated the TSDB/MWCNTs/PGE for Pb(II) measurement. H^1-NMR, C^{13}-NMR and FTIR spectroscopy were used to study the TSDB ligand characteristics. The electrodes modified with PGE, MWCNTs/PGE and TSDB/MWCNTs/PGE were evaluated by cyclic voltammetry (CV) and electrochemical impedance spectroscopy (EIS). Finally, Pb(II) was analysed in wheat grain, cow urine and squid samples using square wave anodic stripping voltammetry (SWASV) with TSDB/MWCNTs/PGE in acetate buffer solution. This was the electrochemical application of the sensor. Atomic absorption spectroscopy (AAS) was used to validate the results of SWASV of the samples.

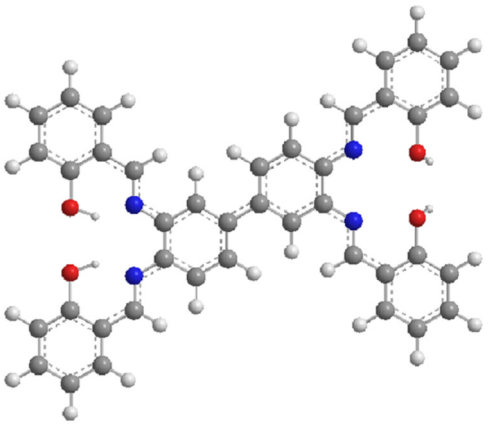

Scheme 1 Synthesis of *N*,*N*′,*N*″,*N*‴-tetrasalicylidene-3,3′-diaminobenzidine (TSDB).

2. Experimental section

2.1. Reagents

Each reagent used was from the explanatory review, and doubly distilled water was used for all the experiments. Salicylaldehyde, 3,3′-diaminobenzidine, 2-aminobenzyl alcohol (assay > 97.5%), lead(II) acetate trihydrate (pure 99%), cadmium acetate dihydrate (extra pure AR, 99%), acetic acid (min. 99.9%), and sodium acetate anhydrous (extra pure AR, 99%) were procured from SRL PVT. Ltd., India. MWCNTs (98% purity) and graphite rods (dia 3 mm) were purchased from Sigma-Aldrich. All the above chemicals and reagents were of analytical grade and were used without further purification.

2.2. Instrumentation or characterization apparatus

Scanning electron microscopy (SEM) and energy dispersive X-ray spectroscopy (EDX) were performed using a Hitachi S3400N (JOEL JSM 6360, with a potential range of 0.3 to 30 kV) instrument. The ^{1}H and ^{13}C NMR spectra were recorded in $CDCl_3$ solution on a Bruker Avance 600 MHz spectrometer. Infrared spectra were recorded on a 650 FT-IR spectrometer (Agilent Technologies). SWASV measurement was carried out using a CHI 660B Analyzer (CH Instruments, USA model). TSDB/MWCNTs/PGE-modified working electrodes were used in conventional three-electrode systems.

2.3. Preparation of the ligand (TSDB)

The *N*′,*N*″,*N*‴-tetrasalicylidene-3,3′-diaminobenzidine (TSDB) ligand (Scheme 2) was produced in the same way as previously reported,[29] with a little change. An ethanolic solution (25 mL) of 3,3′-diaminobenzidine (0.1 mmol) was mixed with salicylaldehyde (0.4 mmol) drop by drop and then refluxed for 3 hours at 60 °C. After cooling the reaction mixture, the yellow compound was filtered, extensively washed with ethanol, recrystallized with methanol, and dried under vacuum.[29]

2.4. TSDB/MWCNT fabrication of paraffin graphite electrodes (PGE)

The fabrication of paraffin graphite electrodes (PGE) is highly sensitive, and the PGE's quality affects the effectiveness of the electrochemical responses as well.[30] First, 0.1 mg of MWCNT material was added to 1 mL of ethanol medium, and the mixture was sonicated for 10 minutes to prepare 0.1 mg mL^{-1} MWCNT dispersion. After that, the PGE (bare electrode) surface was covered with 5 μL of MWCNT suspension, and it was left to dry for 10 minutes. Next, 5 μL of the 1×10^{-3} M ligand was deposited on the MWCNT electrode and allowed to dry for 5 minutes in the air after the TSDB ligand had been dissolved in 0.001 M acetone.

2.5. Voltametric determination of Pb(II)

Pb(II) analysis for the TSDB/MWCNTs/PGE has been examined using SWASV. The TSDB/MWCNTs/PGE was dipped in 0.1 M acetate buffer (pH = 5.5) solution and preconcentrated at 20 μg L^{-1} Pb(II) for 180 s while being mechanically stirred in order to perform the Pb(II) detection. After the modified electrode was placed in a freshly prepared 0.1 M acetate buffer

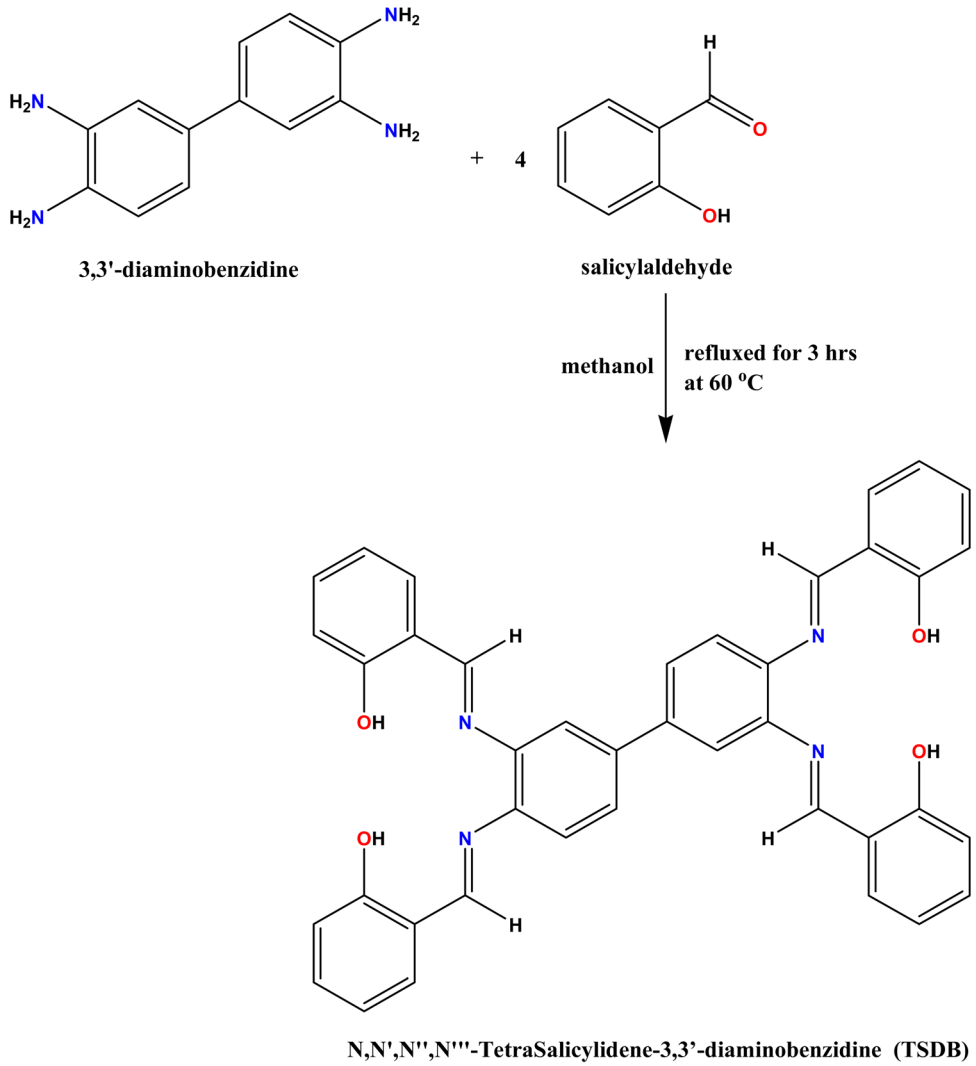

Scheme 2 Synthesis of *N*′,*N*″,*N*‴-tetrasalicylidene-3,3′-diaminobenzidine (TSDB).

(pH = 5.5), the metal ions on the electrode surface were reduced for 90 s at −0.2 V. From a potential range of −0.2 to 0.6 V, the reduced metals on the surface of the TSDB/MWCNTs/PGE were oxidized. The modified electrode was regenerated using 0.01 M ethylene diaminetetraacetic acid (EDTA) for 240 seconds. An explanation is provided for Pb(II)-TSDB/MWCNTs/PGE.

2.6. Preparation of standard solutions

A stock solution of 1 mM Pb(II) was dissolved in pH-5.5 acetate buffer. The stock solution was prepared by successive dilution using 10 mM solutions of Pb(II) in acetate buffer. Pb(II) in the quantity of 0.05 μL was added to known volumes of acetate buffer solutions.

2.7. Real sample preparation

Samples of wheat grains (sample A), cow urine (sample B) and squid (sample C) were brought in from India. The squid samples (sample-C) were first thoroughly cleaned with DD water and then dried at 60 °C in an oven before being ground into a powder. Samples A, B, and C were all mixed with 0.1 mM Pb(II) to prepare stock solutions for the subsequent experiment. Then, SWASV is utilized to analyze Pb(II) in these samples, and the results are compared to those of AAS.

3. Results and discussion

3.1. Characterization of the TSDB ligand

The *N*,*N*′,*N*″,*N*‴-tetrasalicylidene-3,3′-diaminobenzidine (TSDB) ligand was confirmed by Fourier transform infrared (FT-IR) spectroscopy, proton- nuclear magnetic resonance (H^1-NMR) spectroscopy and C^{13}-nuclear magnetic resonance (^{13}C-NMR) spectroscopy.

3.1.1. Fourier transform infrared (FT-IR) spectroscopy. The FT-IR spectra of the TSDB ligand were collected in the 600–4000 cm^{-1} range to confirm the presence of hydroxyl and imino nitrogen groups in the produced ligand. The FT-IR spectra of the TSDB ligand are displayed in Fig. 1. The significant absorption at 3385 cm^{-1} was attributable to the presence of a hydroxyl group. The absorption peaks at

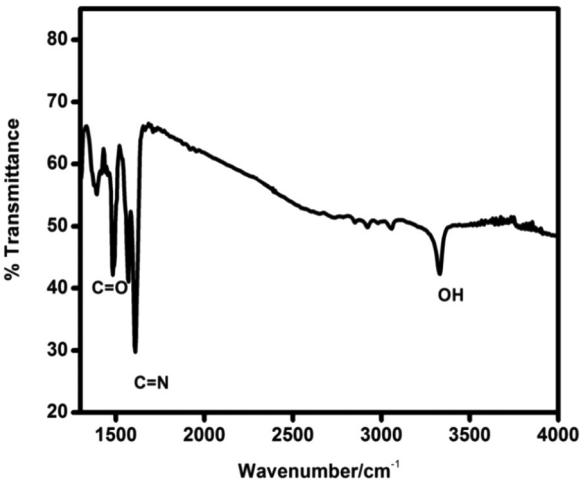

Fig. 1 FT-IR characterization of TSDB.

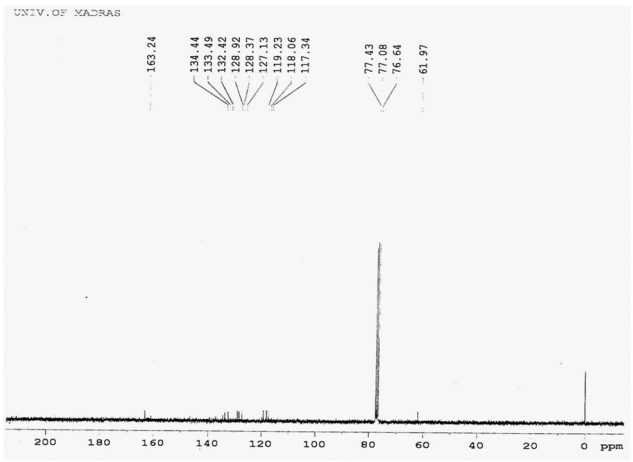

Fig. 3 C^{13}-NMR spectrum of TSDB.

1620 cm^{-1} and 1276 cm^{-1} indicated the presence of the C═N and C–O groups, respectively. The results revealed the presence of hydroxyl and imino nitrogen groups in the synthesized ligand, and the production of the ligand was validated by the FT-IR spectra. These results are also consistent with earlier studies.[29]

3.1.2. ^{1}H-NMR and ^{13}C-NMR spectroscopy. The chemical structure of the synthesized TSDB ligand was determined by ^{1}H-NMR and ^{13}C-NMR spectroscopy. The ^{1}H-NMR and ^{13}C-NMR spectra of the ligand in $CDCl_3$ are illustrated in Fig. 2 and Fig. 3, respectively.[29] ^{1}H-NMR (300 MHz, $CDCl_3$): 11.023 (s, 1*H*), 9.899 (s, 1*H*), 8.615 (s, 3*H*), 7.574–7.259 (m, *J* = 12 Hz, 21*H*), 7.162–6.709 (m, *J* = 12 Hz, 17*H*), 4.871 (s, 4*H*), 4.681 (s, 2*H*).^{13}C-NMR (300 MHz, $CDCl_3$): 163.24, 134.44, 133.49, 132.42, 128.92, 128.37, 127.13, 119.23, 118.06, 117.34, 61.97.

3.2. PGE, MWCNTs/PGE, and TSDB/MWCNTs/PGE characterization

3.2.1. SEM analysis utilizing EDX. The surface morphology of PGE, MWCNTs/PGE, TSDB/MWCNTs/PGE and (Pb(II)-TSDB)/MWCNTs/PGE was identified by SEM and EDX analysis (Fig. 4). The SEM image of the PGE shows a smooth surface (Fig. 4A).

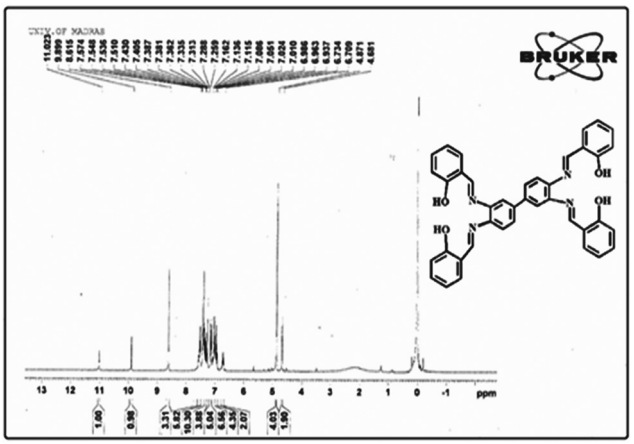

Fig. 2 H^{1}-NMR spectrum of TSDB.

EDX indicates the peak presence of C elements (Fig. 4E). In Fig. 4B, the MWCNTs/PGE image shows the tube-like structure and EDX showed that the intensity of C increases (Fig. 4F). In Fig. 4C, the TSDB/MWCNTs/PGE showed the development of a needle-shaped structure on the electrode's PGE surface, and in Fig. 4G, EDX results show the intense peaks for C, N and O. The (Pb(II)-TSDB)/MWCNTs/PGE results show the intense peaks attributed to Pb, C, N and O (Fig. 4H), and the cloud-shaped structure resulting from Pb(II) adsorption on the TSDB/MWCNTs/PGE surface is shown in Fig. 4D.

3.2.2. Electrochemical behaviour of the PGE, MWCNTs/PGE and TSDB/MWCNTs/PGE. Cyclic voltammetry was utilized to investigate the electrochemical behavior of the modified electrode surface, and $[Fe(CN)_6]^{3-/4-}$ was utilized as a redox probe. The CVs of bare PGE, modified MWCNTs/PGE, and TSDB/MWCNTs/PGE are displayed in Fig. 5A with 1 mM $[Fe(CN)_6]^{3-/4-}$ containing 0.1 M ABS (pH = 5.5). The TSDB/MWCNTs/PGE modified electrode (ΔE_p = 140 mV) was compared with the separation values (ΔE_p = 230 mV and 180 mV) of the naked PGE and MWCNTs/PGE modified electrode, respectively (Table 1). Because of the increased peak potential separation, the bare PGE and MWCNTs/PGE had greater ΔE_p values as compared to the TSDB/MWCNTs/PGE modified electrode. The TSDB/MWCNTs/PGE modified electrode was considered to have lower electrical conductivity, but the bare PGE and MWCNTs/PGE modified electrodes displayed greater ΔE_p values due to an increase in peak potential separation.

Additionally, by adding MWCNTs to bare PGE, the peak current (I_{pa}) was raised from 58 μA to 83 μA. According to the above, a strong and well-defined peak rises at 208 μA for TSDB/MWCNTs/PGE. The much improved I_{pa} values (peak current) of TSDB/MWCNTs/PGE and lower peak potential, or ΔE_p of TSDB/MWCNTs/PGE. The reason for this could be the combination of TSDB/MWCNTs/PGE, which raises the surface area and facilitates electron transport between $[Fe(CN)_6]^{3-/4-}$ and TSDB/MWCNTs/PGE, suggesting a higher level of electrochemical activity.

The square root of the scan rate ($v^{1/2}$) was used to measure the linear increase in the CV peak current in 0.1 M ABS solution

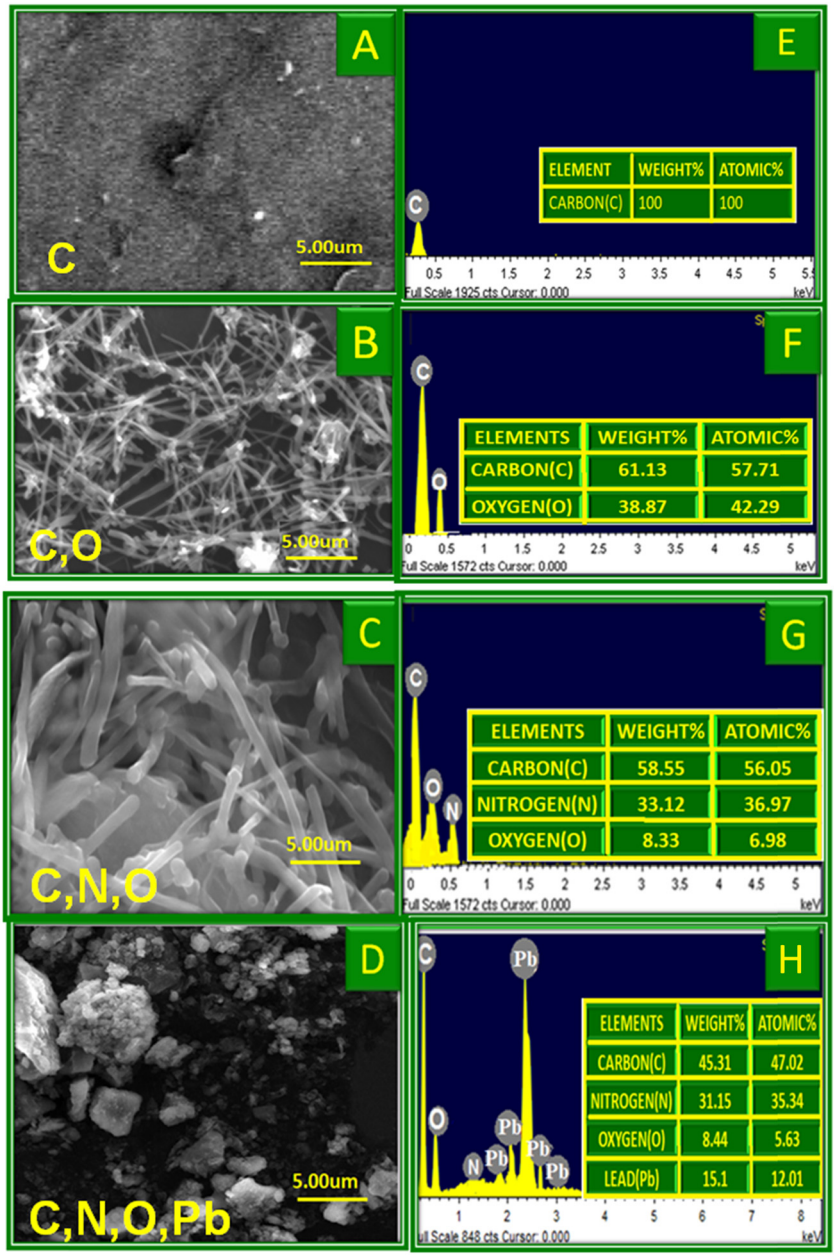

Fig. 4 SEM images of (A) PGE, (B) MWCNTs/PGE, (C) TSDB/MWCNTs/PGE, and (D) [Pb(II)-TSDB]/MWCNTs/PGE and (b) EDAX images of PGE (E), MWCNTs/PGE (F), TSAB/MWCNTs/PGE (G) and [Pb(II)-TSAB]/MWCNTs/PGE (H).

for the TSDB/MWCNTs/PGE. This was due to the electron migration reaction at the modified (TSDB/MWCNTs/PGE) electrode, which is controlled by diffusion.

Using the Randles–Sevcik equation, the active surface area of different electrodes in an irreversible process can be studied.

$$I_p = 2.69 \times 10^5 n^{3/2} A D^{1/2} v^{1/2} C \quad (1)$$

where n is the number of electrons (n = 2), where A is the active electrode surface, D is the diffusion coefficient (7.6×10^{-6} cm^2 s^{-1}), C is the $[Fe(CN)_6]^{3-/4-}$ concentration (1 mM), and v is the scan rate (V s^{-1}). In this equation, n is the number of electrons (n = 2). The calculation of surface area (I_p) of PGE (unmodified electrode), MWCNTs, and TSDB/MWCNTs/PGE (modified electrode), it was noticed that for unmodified electrodes, the I_p value is 0.020 cm^2 and for modified electrodes of MWCNTs, it is 0.090 cm^2, and for TSDB/MWCNTs/PGE, it is 0.150 cm^2. The I_p values of both electrodes are provided in Table 1. Among the above two electrodes, the I_p values of modified electrodes have a high surface area that correlates with that of the unmodified electrode. The obtained result indicates a significant increase in the electroactive surface area of the TSDB/MWCNTs/PGE, up to ~19 times higher than that of the MWCNTs/PGE and PGE.

3.2.3. Electrochemical impedance spectroscopy studies. Fig. 4b shows the results of electrochemical impedance spectroscopy (EIS) measurements in a 1 mM $[Fe(CN)_6]^{3-/4-}$ complex containing 0.1 M KCl solution throughout a frequency range of

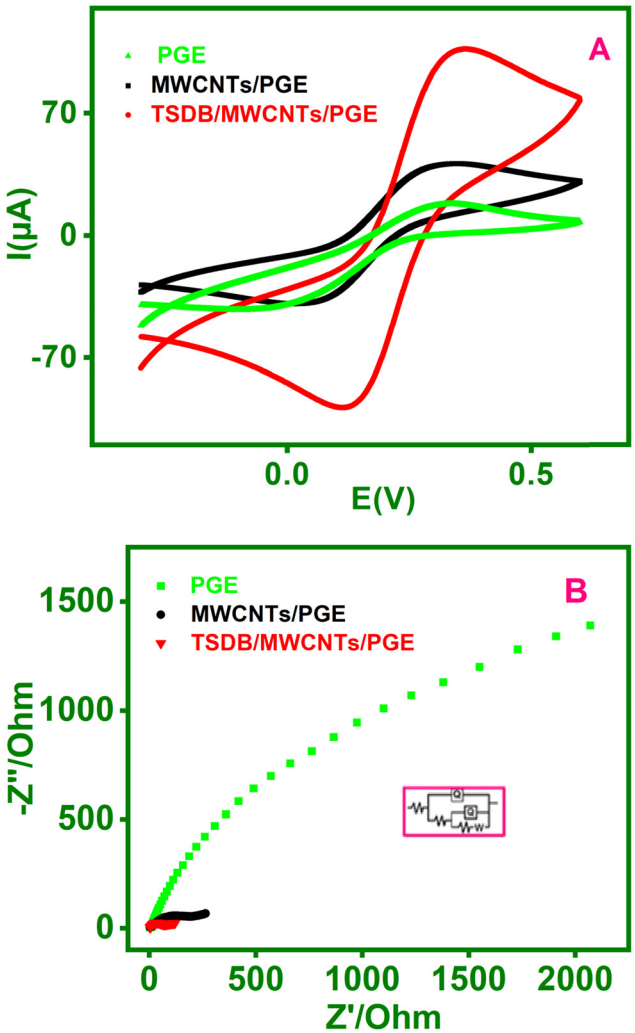

Fig. 5 (A) Cyclic voltammetry for PGE (green line), MWCNTs/PGE (black line) and TSDB/MWCNTs/PGE (red line) and (B) electrochemical impedance spectra obtained for PGE (red line), MWCNTs/PGE (green line) and TSDB/MWCNTs/PGE (blue line) in 1 mM $[Fe(CN)_6]^{3-/4-}$ containing 0.1 mol L^{-1} ABS (pH = 5.5) at 50 mV s^{-1}. Inset: Enlarged image of (B) depicting the EIS results of the TSDB/MWCNT modified electrode.

0.1 Hz to 1.0 MHz. The semicircle portion of the Nyquist figure represents the charge transfer resistance (R_{ct}) at higher frequencies, whereas the linear portion at lower frequencies depicts a diffusion-limited process. Moreover, the resistance solution (R_s) values for modified electrodes with PGE, MWCNTs/PGE, and TSDB/MWCNTs/PGE are 52.36 Ω, 38.16 Ω, and 23.4 Ω, respectively. The R_{ct} was measured at 7490 Ω for the PGE bare electrode, 917.2 Ω for the MWCNTs/PGE, and 194.83 Ω for the TSDB/MWCNTs/PGE modified electrode. The inset (Fig. 5B) displays the schematic depiction of the modified Randle's equivalent circuit for the modified electrode made of TSDB and MWCNTs/PGE. The charge transfer from the circuit is represented by R_{ct}, the resistance solution by R_s, and the Warburg and Cdl capacitance by W. It is clear that the modified electrode made of TSDB/MWCNTs/PGE and MWCNTs/PGE has a lower R_{ct} than the electrode made of PGE, which supports the modified electrode's superior conductivity.

The (σ) electrode conductance (2) was calculated for both the TSDB/MWCNTs/PGE modified and the MWCNTs/PGE modified electrodes in eqn (2).

$$\sigma = \frac{l}{A} \times \frac{1}{R} \quad (2)$$

where the electrodes (MWCNTs/PGE and TSDB/MWCNTs/PGE modified working electrodes) are measured for length (l), surface area (A), and resistance (R). Eqn (2) may be used to calculate the electrode conductivity for PGE, which is 165 × 10^{-5} S cm^{-1}, MWCNTs/PGE, which is 232 × 10^{-5} S cm^{-1} and the modified electrode for TSDB/MWCNTs/PGE, which is 404.3 × 10^{-5} S cm^{-1}. As a result, the modified electrode made of TSDB/MWCNTs/PGE has a greater conductivity than MWCNTs. Consequently, the outcome shows that the TSDB/MWCNTs/PGE had faster electron transfer kinetics and higher conductivity.

Using eqn (3), the phase degree was determined.

$$\phi = \tan^{-1}\left[\frac{1}{1 + 2R_s/R_{ct}}\right] \quad (3)$$

According to the equation, the PGE (bare electrode) phase degree (ϕ) was 42.3°, that of the MWCNTs/PGE was 35.1°, and that of the estimated TSDB/MWCNTs/PGE was 27.0°. Phase angle (ϕ) is directly proportional to (R_{ct}) in accordance with eqn (3). It has improved the electron transfer kinetics at the electrode interface and led to a decrease in the phase angles at the TSDB/MWCNTs/PGE modified electrode. This modified electrode for TSDB/MWCNTs/PGE was therefore appropriate for stripping analysis.

3.2.4. Pb(II) quantification utilizing electrochemical methods. Using cyclic voltammetry, Pb(II) on PGE (bare electrode), (TSDB/MWCNTs/PGE) and MWCNTs/PGE modified electrode was investigated (Fig. 6). For the preconcentration procedure, the modified electrodes were dipped in 0.1 M acetate buffer containing 25 μg L^{-1} of Pb(II) for 180 seconds. After that, the

Table 1 Parameters of PGE, MWCNTs/PGE, and TSDB/MWCNTs/PGE using CV and EIS

Characterization	Terms	PGE	MWCNTs	TSDB/MWCNTs
CV	I_P	0.020 cm^2	0.090 cm^2	0.150 cm^2
	I_{pa} (μA)	58 μA	83 μA	208 μA
	ΔE_P	230 mV	180 mV	140 mV
EIS	R_s	52.36 Ω	38.16 Ω	23.4 Ω
	R_{ct}	7490 Ω	917.2 Ω	194.83 Ω
	σ	165 × 10^{-5} S cm^{-1}	232 × 10^{-5} S cm^{-1}	404.3 × 10^{-5} S cm^{-1}
	θ	42.3	35.1°	27.0°

TSDB/MWCNTs/PGE was washed and placed in a fresh 0.1 M acetate buffer. As a result of CV, there is a good redox peak correlation between MWCNTs and the preconcentrated Pb(II)-TSDB/MWCNTs/PGE. The well-represented redox signal for Pb(II) in Fig. 6A verifies the metal ions' selectivity.

Fig. 6B displays an investigation of the various electrodes of PGE, MWCNTs/PGE and TSDB/MWCNTs/PGE for Pb(II) measurement using square wave anodic stripping voltammetry (SWASV). Preconcentration step-1, a 20 μg L^{-1} of Pb(II) applied by the dipping the electrode into a 0.1 M acetate buffer solution (pH = 5.5) while it was stirred for 180 s owing to the formation of a metal complex. Subsequently, reduction step-2 proves that the metal Pb(II) reduced to Pb(0) at a potential of −1.2 V for 90 s. In stripping step-3, Pb(0) was oxidized to Pb(II) and was stripped off the electrode into the solution by applying a positive direction potential between −1.2 and −0.2 V. As a result, the stripping peak current for Pb(II) was higher on the TSDB/MWCNTs/PGE modified electrode than it was on the MWCNTs/PGE. It was therefore established that the TSDB ligand, present on the surface of the MWCNTs/PGE and used to stabilize the electrode, absorbed metal ions from the preconcentrated medium. The TSDB ligand is composed of four nitrogen groups and a hydroxyl group that are coordinated with metal ions. As a result, TSDB/MWCNTs/PGE increased Pb(II) sensitivity. Scheme 3 shows the mechanism of the Pb(II)-TSDB/MWCNTs/PGE modified electrode.

3.2.5. Supplementary medium pH and preconcentration time effects. The following parameters, including the influence of pH, preconcentration time, and variety of supporting electrolytes, were investigated according to the stripping voltammetric detection of Pb(II), and the obtained findings are shown in Fig. 7.

The stripping voltammogram for Pb(II) was examined after being preconcentrated from different media in 0.1 M acetate buffer (ABS), KNO_3, NH_4NO_3, and $NaNO_3$ solutions. Fig. 7A presents the measured findings for 25 μg L^{-1} of Pb(II) for various electrolytes. In an acetate buffer medium, a greater stripping current response was found. As a result, Pb(II) was determined using 0.1 M acetate buffer medium in the following experiments.

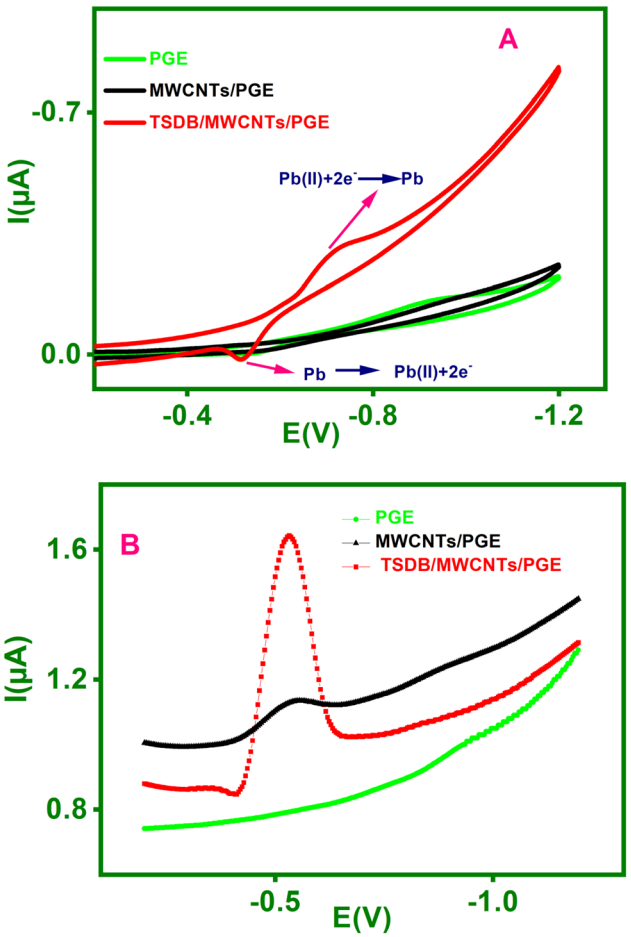

Fig. 6 CV (A) for PGE (green line), MWCNTs/PGE (Black line) and TSDB/MWCNTs/PGE (red line) and SWASV (B) performed on PGE (green line) MWCNTs/PGE (black line) and TSDB/MWCNTs/PGE (red line) with Pb(II) (25 μg L^{-1}) accumulated on the electrode surface in 0.1 M acetate buffer solution (pH 5.5).

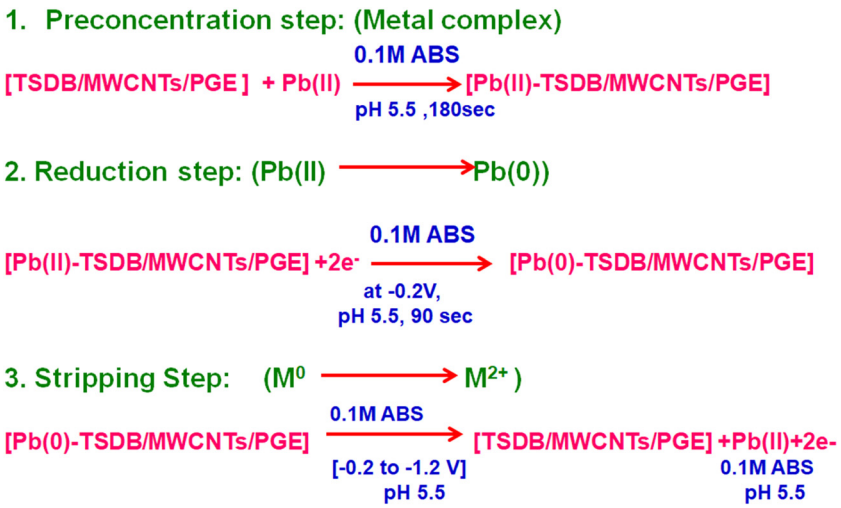

Scheme 3 Mechanism of the Pb(II)-TSDB/MWCNTs/PGE modified electrode.

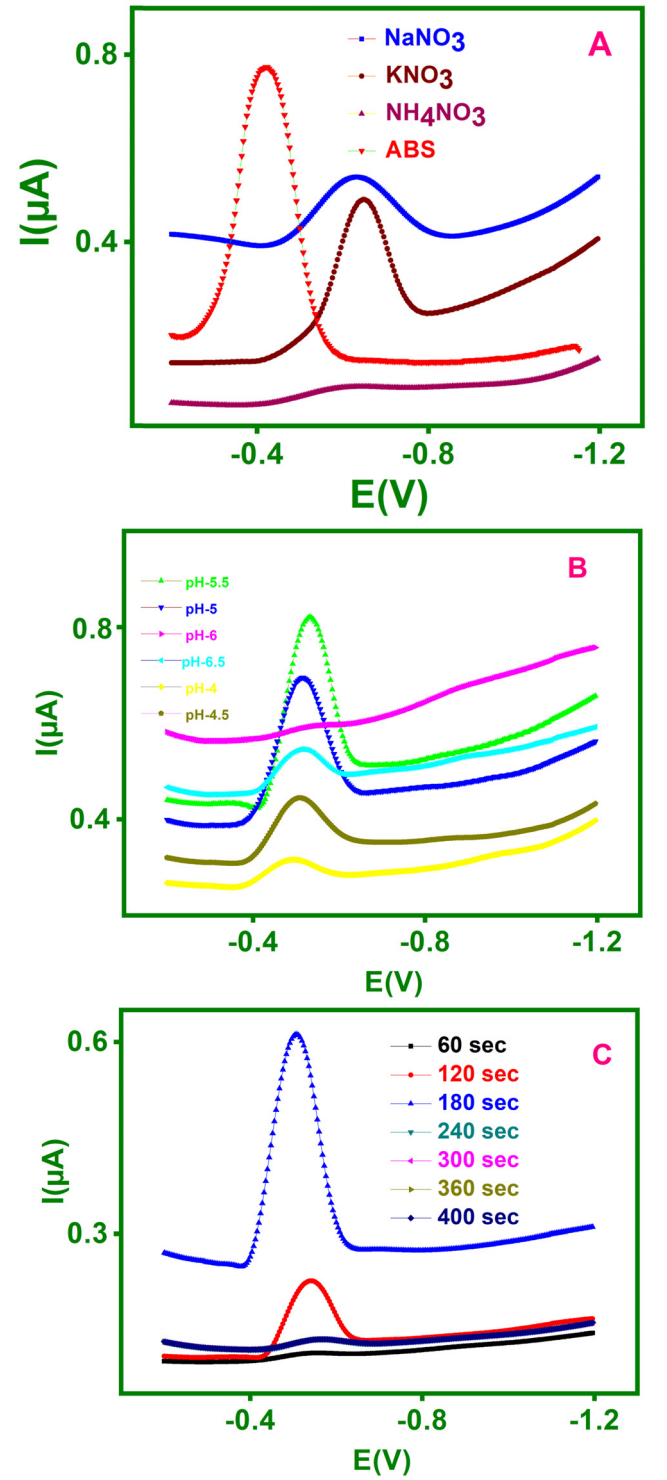

Fig. 7 Effect of (A) the supporting electrolyte (B) pH and (C) preconcentration time on the anodic stripping peak currents of Pb(II) (25 μg L^{-1} each) to evaluate TSDB/MWCNTs/PGE sensor performance in 0.1 M ABS (pH 5.5).

The analysis examined the effect of pH on the anodic stripping current during the preconcentration of 25 μg L^{-1} Pb(II) in 0.1 M acetate buffer. Fig. 7B shows the changes in the stripping current for Pb(II) at pH values ranging from 4.0 to 6.5. It was found that the ideal pH is 5.5 since this pH has a higher peak current for the Pb(II) ion. For this reason, the following measurements were done at pH 5.5.

SWASV was used to examine the effect of preconcentration on Pb(II) electrochemical sensing. Fig. 7C displays the fluctuation in stripping peak currents of 25 μg L^{-1} of Pb(II) in 0.1 M acetate buffer at various interval times ranging from 60 to 300 s. It is evident from the figure that the stripping peak current increased dramatically for 180 s before somewhat decreasing for 300 seconds. Therefore, it was determined that 180 s was the ideal period to detect Pb(II).

3.2.6. Individual evaluation and calibration representation. Using SWASV, the TSDB/MWCNTs/PGE modified electrode was applied for the various Pb(II) concentrations, ranging from 0.8–222 μg L^{-1}. Fig. 8A shows that the stripping peak currents were observed to increase linearly with an increase in Pb(II) concentration. Fig. 8B provides a calibration graph for Pb(II). For Pb(II), a linear range of 0.8–222 μg L^{-1} was noted, with correlation coefficients (R^2) of 0.99. It is concluded that because of Pb(II) capacity to attach to the surface of the TSDB ligand and MWCNT's tendency to increase the stability of

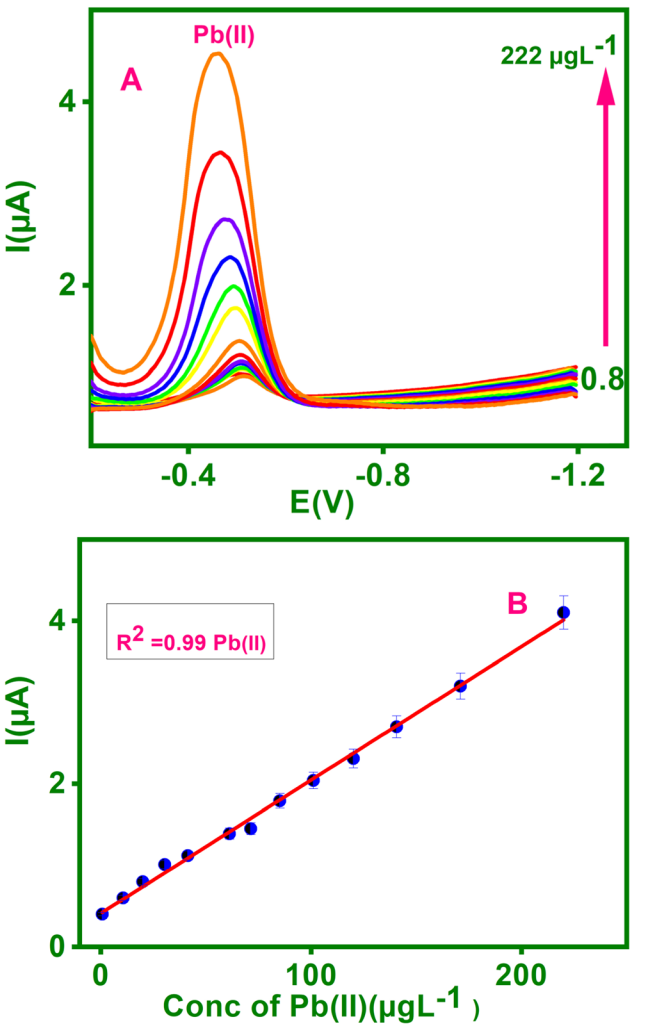

Fig. 8 Determination of Pb(II) by TSDB/MWCNTs/PGE using (A) SWASV corresponding calibration plots for Pb(II) (B) calculated using SWASV.

Table 2 Comparison of TSDB/MWCNTs/PGE for detection of Pb(II) with already reported works

Modified electrode	Linear range (μg L^{-1})	Sensitivity (μA μg L^{-1} cm^{-2})	Detection limit (LOD) (μg L^{-1})	Ref.
GSH/AuNPs/NH2-rGO/GCE	1–120	0.507	0.38	31
ZnO_L-cys/GCE	10 to 140	0.3058	0.397	32
Glu-h-ZnO/GCE	200–18 000	0.0457	42	33
rGO/MoS_2/CS/GCE	5–50	0.311	1.6	34
ZFO/GCE	100–2000	0.1443	5.11	35
(PA/PPy)/ZIF-8@ZIF-67/GCE	20–20 000	0.755	2.9	36
Nb_4C_3Tx/GCE	25–500	0.584	12	37
(BiNCs@AB) composite/GCE	3.0 to 1000	0.91	1.0	38
TSDB/MWCNTs/PGE	0.8–222	0.027	0.15	Our work

Pb(II), the increasing stripping peak current is exactly proportional to mass loading. The equation for linear regression for Pb(II) is as follows: $I_p/\mu A = 0.002x + 0.027$ μg L^{-1} (the sensitivity was 0.027 μA μg L^{-1} cm^{-2}). For Pb(II), the detection limit was found to be 0.15 μg L^{-1}. As a result, a sensitive anodic stripping technique has been developed to measure Pb(II). Additionally, even at very low concentrations, the TSDB/MWCNTs/PGE modified electrode for measuring Pb(II) exhibits good correlations with previously reported modified electrodes (Table 2).

3.2.7. Analysis of Pb(II) for stability and reproducibility. For the analysis of Pb(II), the reproducible performance of the five distinct TSDB/MWCNTs/PGE modified electrodes was tested. Fig. 9A shows the electrodes submerged in 0.1 M acetate buffer at pH 5.5 for 50 μg L^{-1} Pb(II). For Pb(II), the RSD of the electrodes was 1.5%, indicating that the five TSDB/MWCNTs/PGE that were constructed have excellent, dependable, and repeatable performance.

By storing the modified electrode made of TSDB and MWCNTs at room temperature and analyzing 50 μg L^{-1} of Pb(II) using SWASV over one week, the stability of the electrode was evaluated (Fig. 9B). With a standard variation of 1.0% and 99.1% of its initial peak current response, the electrode recorded a significantly reduced stripping peak current of Pb(II). The outcome verified the suggested electrodes' long-term stability for electrochemical use.

3.2.8. Interference studies of metal ions. The investigation of the TSDB/MWCNT's/PGE selectivity for the detection of Pb(II) involved adding 25 μg L^{-1} of interfering metals, such as As(III),

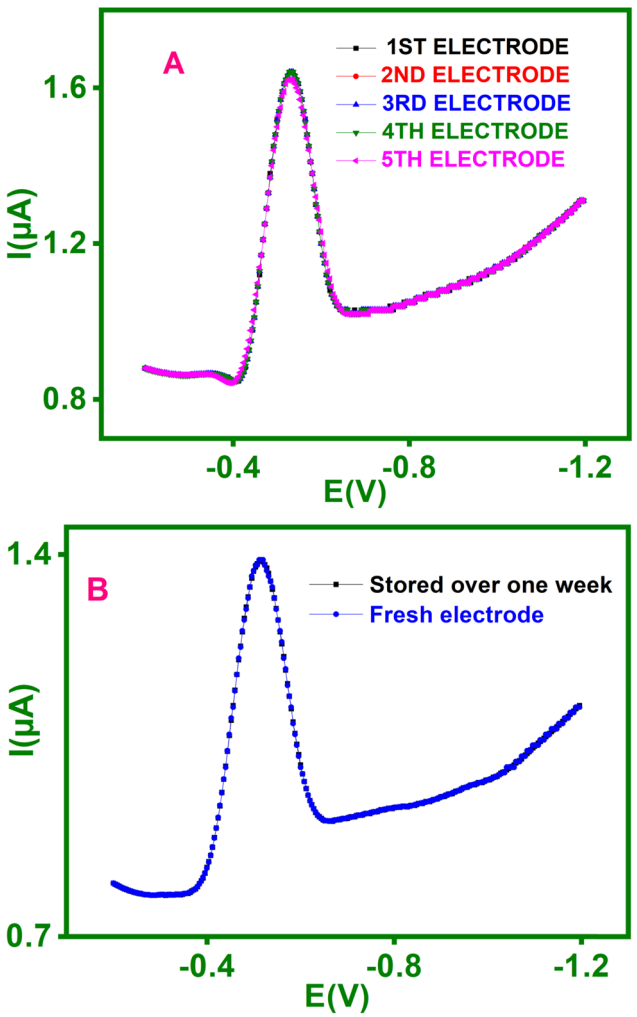

Fig. 9 Stability and reproducibility of the TSDB/MWCNTs/PGE. (A) SWASV curves continuously recorded with six TSDB/MWCNTs prepared under the same conditions in a solution containing 50 μg L^{-1} of Pb(II). (B) Square wave anodic stripping voltammograms of 50 μg L^{-1} of Pb(II) using a freshly prepared electrode (blue line) and one stored at room temperature over one month (black line).

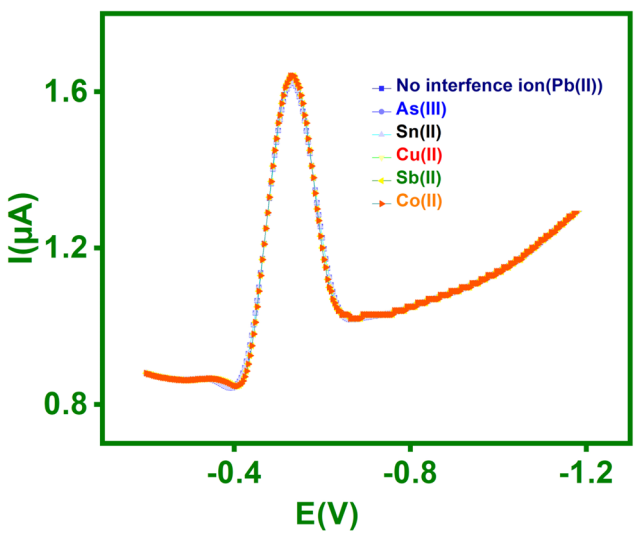

Fig. 10 SWASV curves of the TSDB/MWCNTs/PGE in pH-5.5 ABS containing 50 μg L^{-1} Pb(II) in the presence of 25 μg L^{-1} As(III), Sn(II), Cu(II), Sb(II), and Co(II).

Table 3 Results for Pb(II) in the presence of various interfering ions, As(III), Sn(II), Cu(II), Sb(II) and Co(II), for containing 0.1 M ABS solutions spiked with 50 μg L^{-1} Pb(II)

	Pb(II)	
Interference ions	Peak current (μA)	Relative signal changes (%)
No interference ions	1.64	—
As(III)	1.62	−1.2
Sn(II)	1.61	−1.8
Cu(II)	1.58	−3.6
Sb(II)	1.60	−3.0
Co(II)	1.59	−2.4

Sn(II), Cu(II), Sb(II), and Co(II) in 0.1 M pH-5.5 acetate buffer containing 50 μg L^{-1} of Pb(II). The results are shown in Fig. 10, which shows the stripping peak currents of Pb(II) in the presence (I_i) and in the absence (I_0) of interfering As(III), Sn(II), Cu(II), Sb(II), and Co(II) as well as relative signal changes according to eqn (4).

$$\mathrm{RSD} = \frac{I_i}{I_0 - 1} \quad (4)$$

The RSD values were calculated using the formulae and are displayed in Table 3. The data shown in Table 3 demonstrated that peak currents of Pb(II) had a minor decrease in RSD values by 1.2, 1.8, 3.6, 3.0, and 2.4% when interfering metals such as As(III), Sn(II), Cu(II), Sb(II), and Co(II) were present. As a result, the newly proposed electrode for Pb(II) detection shows superior interference studies.

3.2.9. Analysis of real samples containing Pb(II). Pb(II) in newly prepared wheat grain, cow urine and squid samples is examined, respectively, to determine the precision of the proposed sensor. The wheat grain (sample-A), cow urine (sample-B) and squid (samples-C) samples were taken from India. Samples with varying concentrations of wheat grains (Fig. 11A), cow urine (Fig. 11B) and squid (Fig. 11C) samples were diluted with 0.1 M acetate buffer medium (pH = 5.5), and the results of stripping voltammetry for Pb(II) were recorded. Table 4 displays the recovery outcomes. Good recoveries for Pb(II) were noted in the samples (99.2 to 110%). Sample results were validated against those acquired using AAS. As a result, the constructed sensor demonstrated a reasonable recovery for Pb(II) detection in various samples. It demonstrates that the suggested sensor has excellent precision in detecting Pb(II) in samples A, B, and C.

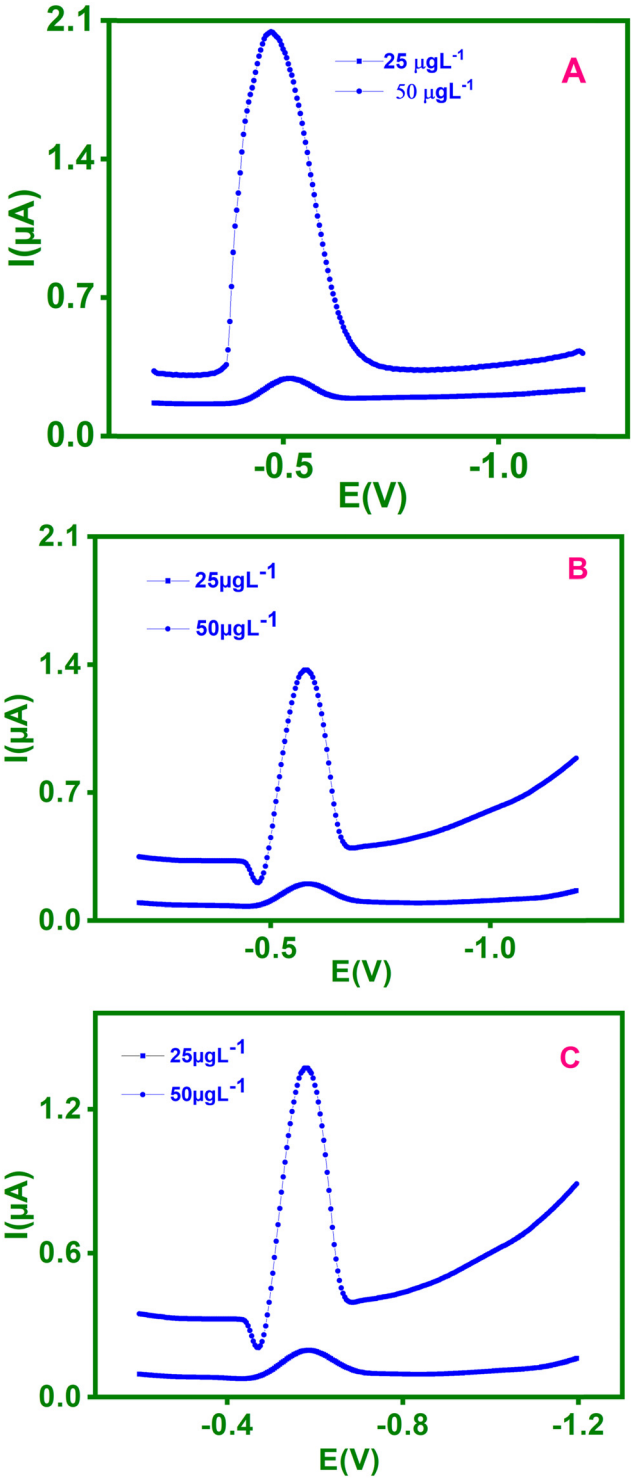

Fig. 11 SWASV of the TSDB/MWCNTs/PGE in pH-5.5 ABS containing 25 μg L^{-1} and 50 μg L^{-1} mixture of Pb(II) at an E_{acc} of −1.2 V and a t_{acc} of 180 s in few environmental samples, wheat grain (a), cow urine (b) and squid (c) samples.

4. Conclusion

Utilizing SWASV, the suggested SDA/MWCNTs/PGE approach analyzes Pb(II). Using SWASV, Pb(II) in wheat grain, cow urine and squid samples was evaluated by TSDB/MWCNTs/PGE. Pb(II) showed a robust recovery, rising from 99.2 to 110%. AAS results and these values were associated. Pb(II) stripping voltammetry observations ranged from 0.8–222 μg L^{-1}, with correlation coefficients (R^2) of 0.99, LODs of 0.15 μg L^{-1}, and sensitivity values of 1.141 μA μg^{-1} L^{-1} cm^{-2}. The stripping current peak for Pb(II) was stable, and the stability of the TSDB/MWCNTs/PGE was recorded for both the new electrode and the original electrode. According to anti-interference tests, the stripping peak of Pb(II) with less than ±5% inaccuracy does

Table 4 Comparison of the present method and AAS for analysis of Pb(II) (n = 3)

		Square wave anodic stripping voltammetry (SWASV)				Atomic absorption spectroscopy (AAS)	
Samples	Metal ions	Added (μg L^{-1})	Found (μg L^{-1})	RSD (%)	Recovery (%)	Found (μg L^{-1})	Recovery (%)
Sample-A	Pb(II)	25.0	24.8	1.3	99.4	30.0	100.0
(Wheat grains)		50.0	56.0	1.7	102.0	60.0	100.0
Sample-B	Pb(II)	25.0	25.3	2.0	101.0	27.0	102.0
(Cow urine)		50.0	56.3	2.1	102.3	55.0	103.0
Sample-C	Pb(II)	25.0	27.0	2.5	108.0	33.0	105.0
(Squid)		50.0	55.0	2.7	110.0	65.0	107.0

not alter when compared to other metal ions that have been measured. Ultimately, it was shown that a newly synthesized TSDB/MWCNTs/PGE significantly increased the sensitivity of Pb(II).

Data availability

The data used to support the findings of this study are included within the article.

Conflicts of interest

There are no conflicts to declare.

Acknowledgements

The authors are very thankful to the Dean R & D and University Management Committee Members of Vel Tech Rangarajan Dr Sagunthala R & D Institute of Science and Technology, Avadi, Chennai, for providing the necessary instrumental facilities to carry out the research work.

References

1 S. Palisoc, E. T. Lee, M. Natividad and L. Racines, Silver nanoparticle modified graphene paste electrode for the electrochemical detection of lead, cadmium and copper, *Int. J. Electrochem. Sci.*, 2018, **13**(9), 8854–8866.
2 M. O. C. Ogwuegbu and W. Muhanga, Investigation of lead concentration in the blood of people in the copper belt province of Zambia, *J. Environ.*, 2005, **1**, 66–75.
3 M. Wińska-Krysiak, K. Koropacka and S. Gawroński, Determination of the tolerance of sunflower to lead-induced stress, *J. Elem.*, 2015, **20**(2), 491–502.
4 S. Kumar, R. Islam, P. B. Akash, M. H. R. Khan, R. Proshad, J. Karmoker and G. R. MacFarlane, Lead (Pb) contamination in agricultural products and human health risk assessment in Bangladesh, *Water, Air, Soil Pollut.*, 2022, **233**(7), 257.
5 A. Kushwaha, N. Hans, S. Kumar and R. Rani, A critical review on speciation, mobilization and toxicity of lead in soil-microbe-plant system and bioremediation strategies, *Ecotoxicol. Environ. Saf.*, 2018, **147**, 1035–1045.
6 S. Xiong, B. Yang, D. Cai, G. Qiu and Z. Wu, 2015. Individual and simultaneous stripping voltammetric and mutual interference analysis of Cd^{2+}, Pb^{2+} and Hg^{2+} with reduced graphene oxide-Fe_3O_4 nanocomposites, *Electrochim. Acta*, 2015, **185**, 52–61.
7 T. E. Novotny, S. A. Bialous, L. Burt, C. Curtis, V. L. D. Costa, S. U. Iqtidar, Y. Liu, S. Pujari and E. Tursan d'Espaignet, The environmental and health impacts of tobacco agriculture, cigarette manufacture and consumption, *Bull. W. H. O.*, 2015, **93**, 877–880.
8 D. C. Bellinger, The protean toxicities of lead: new chapters in a familiar story, *Int. J. Environ. Res. Public Health*, 2011, **8**(7), 2593–2628.
9 G. Flora, D. Gupta and A. Tiwari, Toxicity of lead: a review with recent updates, *Interdiscip. toxicol.*, 2012, **5**(2), 47–58.
10 Z. Fang, J. Růžička and E. H. Hansen, An efficient flow-injection system with on-line ion-exchange preconcentration for the determination of trace amounts of heavy metals by atomic absorption spectrometry, *Anal. Chim. Acta*, 1984, **164**, 23–39.
11 P. P. Gao, X. M. Zhang, P. Y. Xue, J. W. Dong, Y. Dong, Q. L. Zhao, L. P. Geng, Y. Lu, J. J. Zhao and W. J. Liu, Mechanism of Pb accumulation in Chinese cabbage leaves: Stomata and trichomes regulate foliar uptake of Pb in atmospheric PM2.5, *Environ. Pollut.*, 2022, **293**, 118585.
12 K. Kocot and R. Sitko, Trace and ultratrace determination of heavy metal ions by energy-dispersive X-ray fluorescence spectrometry using graphene as solid sorbent in dispersive micro solid-phase extraction, *Spectrochim. Acta, Part B*, 2014, **94**, 7–13.
13 M. A. Habila, Z. A. ALOthman, A. M. El-Toni and M. Soylak, Combination of syringe–solid phase extraction with inductively coupled plasma mass spectrometry for efficient heavy metals detection, *CLEAN:Soil, Air, Water*, 2016, **44**(6), 720–727.
14 D. Manivannan and V. M. Biju, Determination of toxic heavy metals in sea water by FAAS after preconcentration with a novel chelating resin, *Water Sci. Technol.*, 2011, **64**(4), 803–808.
15 AOAC International, E. W. Sydenham, G. S. Shephard, P. G. Thiel, S. Stockenström, P. W. Snijman, D. J. Van Schalkwyk and Collaborators, *J. AOAC Int.*, 1995, **78**, 688–696.
16 T. Priya, N. Dhanalakshmi and N. Thinakaran, Electrochemical behavior of Pb (II) on a heparin modified chitosan/graphene nanocomposite film coated glassy carbon electrode and its sensitive detection, *Int. J. Biol. Macromol.*, 2017, **104**, 672–680.
17 S. Xiong, S. Ye, X. Hu and F. Xie, Electrochemical detection of ultra-trace Cu (II) and interaction mechanism analysis

between amine-groups functionalized $CoFe_2O_4$/reduced graphene oxide composites and metal ion, *Electrochim. Acta*, 2016, **217**, 24–33.

18 H. Ge and X. Fan, Adsorption of Pb^{2+} and Cd^{2+} onto a Novel Activated Carbon-Chitosan Complex, *Chem. Eng. Technol.*, 2011, **34**(10), 1745–1752.

19 T. Yan, Z. Wang and Z. J. Pan, Flexible strain sensors fabricated using carbon-based nanomaterials: A review, *Curr. Opin. Solid State Mater. Sci.*, 2018, **22**(6), 213–228.

20 A. Sinha, Dhanjai, R. Jain, H. Zhao, P. Karolia and N. Jadon, Voltammetric sensing based on the use of advanced carbonaceous nanomaterials: a review, *Microchim. Acta*, 2018, **185**, 1–30.

21 J. Xu, Z. Cao, Y. Zhang, Z. Yuan, Z. Lou, X. Xu and X. Wang, A review of functionalized carbon nanotubes and graphene for heavy metal adsorption from water: Preparation, application, and mechanism, *Chemosphere*, 2018, **195**, 351–364.

22 C. Guo, C. Wang, H. Sun, D. Dai and H. Gao, A simple electrochemical sensor based on rGO/MoS_2/CS modified GCE for highly sensitive detection of Pb (ii) in tobacco leaves, *RSC Adv.*, 2021, **11**(47), 29590–29597.

23 S. Tajik, A. Lohrasbi-Nejad, P. Mohammadzadeh Jahani, M. B. Askari, P. Salarizadeh and H. Beitollahi, Co-detection of carmoisine and tartrazine by carbon paste electrode modified with ionic liquid and MoO_3/WO_3 nanocomposite, *J. Food Meas. Charact.*, 2022, 1–9.

24 H. Mahmoudi Moghaddam, H. Beitollahi, S. Tajik, I. Sheikhshoaie and P. Biparva, Fabrication of novel TiO_2 nanoparticles/Mn(III) salen doped carbon paste electrode: application as electrochemical sensor for the determination of hydrazine in the presence of phenol, *Environ. Monit. Assess.*, 2015, **187**, 1–12.

25 H. Beitollahi, M. Shahsavari, I. Sheikhshoaie, S. Tajik, P. M. Jahani, S. Z. Mohammadi and A. A. Afshar, Amplified electrochemical sensor employing screen-printed electrode modified with Ni-ZIF-67 nanocomposite for high sensitive analysis of Sudan I in present bisphenol A, *Food Chem. Toxicol.*, 2022, **161**, 112824.

26 S. Tajik, M. A. Taher and H. Beitollahi, The first electrochemical sensor for determination of mangiferin based on an ionic liquid–graphene nanosheets paste electrode, *Ionics*, 2014, **20**, 1155–1161.

27 S. Tajik, Z. Dourandish, F. G. Nejad, H. Beitollahi, P. M. Jahani and A. Di Bartolomeo, Transition metal dichalcogenides: Synthesis and use in the development of electrochemical sensors and biosensors, *Biosens. Bioelectron.*, 2022, **216**, 114674.

28 A. S. Ahmed, M. B. I. Mohamed, M. A. Bedair, A. A. El-Zomrawy and M. F. Bakr, A new Schiff base-fabricated pencil lead electrode for the efficient detection of copper, lead, and cadmium ions in aqueous media, *RSC Adv.*, 2023, **13**(23), 15651–15666.

29 Lallan Mishra, Kumari Bindu and Subrato Bhattacharya, *Indian J. Chem.*, 2004, **43**, 315–319.

30 Jayagopi Gayathri, Sivakumar Sivalingam and Sanglimuthu Sriman Narayanan, Determination of Pb^{2+} and Cd^{2+} ions in raw milk, honey and groundnut shell using TSAB/MWCNT, *Mater. Adv.*, 2023, **4**(250), 2502–2511.

31 Jinbang Mei, *et al.*, A sensitive and selective electrochemical sensor for the simultaneous determination of trace Cd^{2+} and Pb^{2+}, *Chem. Pap.*, 2020, **74**, 1027–1037.

32 Vitor H. B. Oliveira, *et al.*, A sensitive electrochemical sensor for Pb^{2+} ions based on ZnO nanofibers functionalized by L-cysteine, *J. Mol. Liq.*, 2020, **309**, 113041.

33 Lateef Ahmad Malik, *et al.*, Studies on a glutathione coated hollow ZnO modified glassy carbon electrode; a novel Pb(II) selective electrochemical sensor, *RSC Adv.*, 2021, **11**(30), 18270–18278.

34 Chuanen Guo, *et al.*, A simple electrochemical sensor based on rGO/MoS_2/CS modified GCE for highly sensitive detection of Pb(II) in tobacco leaves, *RSC Adv.*, 2021, **11**(47), 29590–29597.

35 Changchun Fan, *et al.*, $ZnFe_2O_4$ nanoparticles for electrochemical determination of trace Hg(II), Pb(II), Cu(II), and glucose, *ACS Appl. Nano Mater.*, 2021, **4**(4), 4026–4036.

36 Wanqing Zhang, *et al.*, Electrochemical determination of lead(II) and copper(II) by using phytic acid and polypyrrole functionalized metal-organic frameworks, *Microchim. Acta*, 2020, **187**, 1–9.

37 P. Abdul Rasheed, *et al.*, Large interlayer spacing Nb_4C_3Tx (MXene) promotes the ultrasensitive electrochemical detection of Pb^{2+} on glassy carbon electrodes, *RSC Adv.*, 2020, **10**(41), 24697–24704.

38 Jin Zou, *et al.*, Bismuth nanoclusters/porous carbon composite: A facile ratiometric electrochemical sensing platform for Pb^{2+} detection with high sensitivity and selectivity, *ACS Omega*, 2021, **7**(1), 1132–1138.